A novel approach to Dielectrophoresis using Carbon Electrodes

Rodrigo Martinez-Duarte[1,2]*, Philippe Renaud*[2] *and Marc J. Madou*[1,3]

[1] Department of Mechanical & Aerospace Engineering, University of California, Irvine, United States of America

[2] École Polytechnique Fédérale de Lausanne, Switzerland

[3] Ulsan National Institute for Science and Technology, World Class University Program, South Korea

Corresponding Author: Dr. Rodrigo Martinez-Duarte, EPFL-STI-LMIS4, Station 17, CH-1015 Lausanne, Switzerland. drmartnz@gmail.com, Fax: +41 21 693 5950

Abbreviations: carbon-DEP, carbon-electrode dielectrophoresis; DEP, dielectrophoresis; CNC, computer numerical control; iDEP, insulator-based DEP; C-MEMS, carbon microelectromechanical systems; PSA, pressure-sensitive adhesive; PC, polycarbonate; FCS, fetal calf sera; BSA, bovine serum albumin; AR, aspect ratio

Keywords: dielectrophoresis, 3D, carbon, high throughput, metal, insulator, cell, filter, sorting

Total number of words: 5,215

Abstract. Carbon-electrode dielectrophoresis is demonstrated here as an alternative to more traditional DEP techniques. Carbon-DEP combines advantages of metal-electrode and insulator-based DEP by using low cost fabrication techniques and low voltages for particle manipulation. The use of 3D electrodes is proved to yield significant advantages over the use of traditional planar electrodes. This paper details the fabrication of dense arrays of tall high aspect ratio carbon electrodes on a transparent fused silica substrate. The shrinkage of the SU-8 structures during carbonization is characterized and a design tool for future devices is provided. Applications of carbon electrodes in DEP are then detailed and include particle positioning, high throughput filtering and cell focusing using positive-DEP. Manipulated cells include *s. cerevisiae* and *drosophila melanogaster*. The advantages and disadvantages of carbon-DEP are discussed at the end of this work.

1 Introduction

Dielectrophoresis (DEP) is a technique for particle manipulation that exploits the interaction between an induced dipole and a non-uniform electric field. Most of the work on DEP has relied on the use of planar metal microelectrodes to create the required non-uniform electric field across a sample. Examples of the use of planar metal-electrodes for DEP include the selective manipulation and sorting of blood cells, cancer cells and microorganisms [1-3]. However, planar electrodes on the channel surfaces only generate an electric field gradient close to the electrode and not throughout the bulk of the solution in the remainder of the fluidic channel. In contrast, the use of 3D electrodes that cover the whole height of the channel allows for the addressing of all particles throughout the solution in the channel. Indeed the use of 3D electrodes minimizes the distance from a targeted particle to the nearest electric field gradient and thus reduces or

eliminates altogether the number of re-flow cycles that may be required to improve throughput when using planar electrodes. Unfortunately, the fabrication of 3D metal electrodes quickly turns complicated and expensive as it typically requires the use of metal electroplating which often limits the yield and results in more expensive devices. Examples on the use of electroplated gold structures for DEP applications include those by Wang, et al [4] who used them for 3D cell focusing and by Voldman, et al [5] who used gold pillars to implement an interrogation site for flow cytometry applications.

An alternative to metal-electrode DEP is insulator-based dielectrophoresis or iDEP [6-8]. In this technique, metal macro electrodes (for example extruded wire rods or machined metal plates) are positioned on both ends of an array of insulating microstructures. A high voltage is then applied to the metal electrodes to create a uniform electric field between them that is rendered non-uniform in the vicinity of the insulator structures. iDEP allows for the low-cost fabrication of experimental devices since 1) no metal micro electrodes are required, 2) the insulator structures, either 2D or 3D, are made of inexpensive materials such as glass or polymer and 3) low-cost fabrication techniques such as injection molding and embossing can be used. Another important advantage of iDEP over metal-electrode DEP is the reduced chance of sample electrolysis since the sample does not necessarily contact the metal electrodes. Unfortunately, iDEP requires very high voltages (electric field magnitude is inversely proportional to the gap between electrodes and in iDEP the separation between metal electrodes can be in the order of centimeters) to create a suitable electric field gradient for DEP which increases the cost of the polarizing electronics and the hazard of electric shock during operation.

Here we present the use of carbon electrodes as an alternative to both metal-electrode DEP and iDEP. Carbon-electrode DEP or carbon-DEP combines the advantages of metal-based and

insulator-based DEP: the fabrication of 3D carbon electrodes is relatively simple and low cost, an advantage shared with iDEP; while low voltages suffice to polarize the carbon electrodes and create an electrical field suitable for DEP, an advantage shared with metal electrodes. Furthermore, 1) carbon has a wider electrochemical stability window than gold and platinum and affords higher applied voltages in a given solution without electrolyzing it [9]. In fact glass-like carbon, also known as glassy carbon[§], is a preferred material among electrochemists due to its remarkable stability [10-14]; 2) glass-like carbon has excellent biocompatibility and has been demonstrated both as an implantable material [15] and as substratum for cell culture [16]; 3) glass-like carbon is also chemically very inert in almost all solvents/electrolytes. Remarkably, it withstands attack from strong acids such as nitric, sulfuric, hydrofluoric or chromic and other corrosive agents such as bromine [17]; and 4) glass-like carbon has good mechanical properties with a hardness of 6 to 7 on Mohs' scale, a value comparable to that of quartz, and a Young's modulus in the range between 10 and 40 GPa (compared to 168 GPa of platinum, 79 GPa of gold and 65-90 GPa for common glass) [18]. Glass-like carbon microelectrodes are derived by the pyrolysis, heating to high temperatures in an inert atmosphere, of a previously shaped organic polymer in a process known as Carbon MEMS (C-MEMS) [9]. Carbonizable polymers are widely available and high-quality ones are typically much less expensive than metals such as gold and platinum used in thin film metal electrode fabrication. The polymer can be shaped using any suitable low cost technique such as photolithography, CNC (computer numerical control) machining, moulding and embossing. No expensive and complex equipment such as metal evaporators or metal sputterers is required. The electrical resistivity of glass-like carbon is close to 1×10^{-4} Ω·m [19] which is higher than that of metals (*i.e.*, Au = 2.44×10^{-8}, Pt = 1.06×10^{-7} Ω·m) but is still low enough to create a suitable electric field gradient for DEP using tens of

volts. Previous work on carbon-DEP by the UC Irvine BIOMEMS team and collaborators includes a yeast viability assay [20], bacterial sorting [21] and the incorporation of carbon-DEP in a centrifugal microfluidics platform [22]. Modeling and simulation work of carbon-DEP has also been carried out [23-25].

The current paper details for the first time the fabrication of dense arrays of high aspect ratio carbon electrodes on fused silica substrates. SU-8 is used as carbon precursor and UV-photolithography is utilized to pattern the SU-8. The characterization of the shrinkage of high aspect ratio SU-8 structures during carbonization is reported and a design tool for future carbon-DEP devices is provided. Different applications of Carbon-DEP are validated and include particle positioning, a high throughput filter and cell focusing using positive-DEP. Manipulated cells include *s. cerevisiae* and *drosophila melanogaster*.

2 Materials and methods

A significant improvement presented in this paper is the fabrication of carbon electrodes on a transparent substrate. Previous work in carbon-DEP only made use of opaque silicon as the substrate material [21, 22, 25]. The carbonization of SU-8 requires temperatures up to 900 °C and thus few materials, transparent or opaque, can be used as substrates. Transparent fused silica is chosen here because of its maximum service temperature of 950 °C and because it is significantly cheaper than other high-temperature transparent materials such as sapphire. The use of a transparent substrate greatly improves the versatility of carbon-DEP devices and makes them more amenable for integration with other systems. For example, the use of fused silica facilitates the rapid, continuous determination of cell concentration in the microchannel using

techniques such as spectrophotometry. A transparent substrate also enables the use of an inverted microscope for experiment visualization.

The complete fabrication process is illustrated in figure 1A. The process starts with the photo-patterning of the carbon precursor on the fused silica substrate (Synthetic silica-ES grade from Tosoh Corporation, Japan). SU-8, a negative photoresist is used in this work as the carbon precursor and was purchased from Gersteltec Sárl, Switzerland. SU-8 photolithography is implemented in two steps: 1) fabrication of planar interdigitated fingers that will become carbon connection leads to the base of the 3D carbon electrodes and 2) fabrication of SU-8 pillars that will become the 3D carbon electrodes. The process parameters to fabricate selected SU-8 structures on fused silica are summarized in table 1. These parameters are optimized to fabricate structures featuring gaps in between them as narrow as 20 μm. Details on the fabrication of carbon electrodes on silicon substrates can be found elsewhere [25]. Important differences on the processing of SU-8 on quartz and silicon exist. The processing of SU-8 on quartz substrates requires the use of lower exposure doses than those used to initiate cross-linking of a SU-8 layer of similar height deposited on silicon. Furthermore, the implementation of a hard bake at 190 °C after the development of the SU-8 structures is crucial to improve the adhesion of SU-8 to fused silica and prevent the SU-8 from peeling off during pyrolysis.

The SU-8 patterns are carbonized in a furnace (ATV Technologies Gmbh PEO601, Germany) under a constant nitrogen gas flow of 2000 $ml \cdot min^{-1}$. The pyrolysis protocol features 2 stages: 1) a temperature ramp from room temperature to 200 °C at 10 $°C \cdot min^{-1}$ followed by a 30 minute dwell at 200 °C to allow for any residual oxygen to be evacuated from the chamber and prevent combustion of the polymer as the temperature is raised further; and 2) a temperature ramp from 200 to 900 °C at 10 $°C \cdot min^{-1}$ with a one-hour dwell at 900 °C to complete carbonization[†]. The

samples are then cooled down to room temperature at a ramp of 10 °C·min^{-1}. Examples of different carbon electrode shapes are shown in figure 1B. Shrinkage occurs during pyrolysis and is detailed in the results section.

After pyrolysis, the carbon electrodes and the areas in between are de-scummed using oxygen plasma (flow rate of 400 ml·min^{-1} and power of 500 W for 30 s in a PVA TEPLA 300 Dry Etcher) to eliminate any carbon residues between the electrodes that could lead to an electrical short-circuit during experiments. A thin layer, ~2 μm, of SU-8 is then patterned around the carbon electrodes to electrically insulate the connection leads and to planarize the surface around the base of the electrodes (fabrication details of this layer are provided in table 1).

The microfluidic network is fabricated separate from the carbon electrodes. The network is fabricated out of pressure-sensitive double-sided adhesive (PSA) and polycarbonate (PC). A microchannel is first cut from a 100 μm-thick PSA (FLEXMOUNT Advantage FAD 100 V, FLEXcon, USA) using a cutter-plotter (Graphtec CE-2000-60, Japan) and is aligned between a couple of 1 mm-diameter holes previously drilled in a PC substrate. The carbon electrode array is then aligned within the channel in the PSA-PC stack. Finally, the PSA is sealed to the thin layer of SU-8 around the base of the electrodes using a laminator (EasyMount 65, VellumArt, England). The cross-section of a typical carbon-DEP device is shown in figure 1A. The inlet and outlet to and from the channel are implemented using commercial connectors (NanoPort™ N-333, Upchurch Scientific, USA) or connectors fabricated in-house.

The shrinkage during carbonization was quantified by measuring and comparing the dimensions of the SU-8 and carbon structures using scanning electron microscopy (Hitachi S-4700-2 FESEM and Carl Zeiss Leo 1550) and surface profilometry (Dektak 3 and Tencor Alpha-step 500).

The use of carbon electrodes in DEP applications is demonstrated using two experimental setups. The first platform is modeled after traditional setups used in DEP experiments and features a syringe infusion pump (Harvard Apparatus PHD2000), a function generator (Agilent 33250A or Stanford Research Systems DS345) and an upright microscope (Nikon Eclipse LV100 or MOTIC PSM1000). External components to the carbon-DEP device include tubing, valves and Y-connectors (Upchurch Scientific parts 1522, P-782 and P-512 respectively) and are used to route the sample from a syringe through the carbon-DEP device and out to collecting vials. The second experimental platform is based on a compact disc-like centrifugal microfluidics platform fabricated in-house. Full fabrication details and the advantages of using this platform over a syringe-based have been previously presented by some of us [22].

Yeast cells (*Saccharomyces cerevisiae*, Sigma-Aldrich), 8 μm-diameter latex particles (Duke Scientific, USA) and *Drosophila melanogaster S2 cells* are used as experimental particles. Yeast cultures were obtained by dissolving 200 mg of yeast in 10 ml sterile YPD medium (MP Biomedicals) and incubated aerobically at 30°C with 150-250 rpm rotation for 18 hours. This culture was then diluted into 100 ml of the equivalent media and incubated as before for a further 24 hours. *Drosophila melanogaster S2* cells were grown overnight at room temperature and dark conditions in 10 ml of Schneider's media (Invitrogen) complemented with 10% fetal calf sera (FCS) from Sigma-Aldrich. The experimental samples used here are summarized in table 2 and were obtained by peleting the appropriate cell culture using centrifugation at 3000-5000 x g for 5-10 minutes and re-suspending the cells in the appropriate experimental media. The sample was then diluted using experimental media until the desired cell concentration was reached. Latex particles are first suspended in experimental media and later mixed at specific ratios with the cell dilution to obtain experimental samples #3 and #4. The addition of bovine serum albumin (BSA)

from Sigma-Aldrich in experimental samples 3 and 5 continuously prevents cell adhesion to the device during experiments. A 0.1% BSA solution was flowed through to pre-treat the devices used with experimental samples not featuring BSA in their composition (samples 1, 2 and 4). Direct counting using a hemacytometer kit with improved Neubauer ruling (Hausser Scientific, USA) is used to quantify the particle and cell concentration in the samples retrieved from the carbon-DEP chip.

3 Results and discussion

3.1 Shrinkage of SU-8 structures during pyrolysis

Structure shrinkage has been previously shown to depend on various factors including the type of polymer used as carbon precursor [26] and amount of cross-linkage in the polymer matrix [27]. The results obtained here when pyrolyzing SU-8 pillars show a shrinkage percentage that is highly dependant on the initial dimensions of the pillars. Cross-linkage in the SU-8 matrix was not quantified. Up to 86% shrinkage is obtained when pyrolyzing features with a height around 10 μm (the resultant carbon is only 1.4 μm-high). Shrinkage decreases as the dimensions of the original SU-8 pillar increase. Heights greater than 300 μm feature a shrinkage as low as 37%. This trend is illustrated in figure 2A. The shrinkage percentage at any given height of the original SU-8 structure is highly repeatable and figure 2A is presented here as a design tool for future carbon-DEP designs. The shrinkage during pyrolysis imposes additional considerations on the fabrication of SU-8 structures that will become carbon electrodes to be used in DEP applications. The DEP force is directly proportional to the squared magnitude of the established electric field gradient between electrodes. The electric field gradient depends on both the voltage used to polarize the electrodes and the gap between them. If the gap between electrodes increases, the

applied voltage must increase accordingly to meet the electric field gradient requirements. Practical DEP devices benefit from the use of low voltage and the gap between electrodes must be kept as narrow as possible. Since SU-8 structures shrink during pyrolysis the gaps between them must be narrower than those desired between carbon electrodes. For example, gaps of 15 μm between two SU-8 pillars of diameter equal to 50 μm and aspect ratio of 4 lead to gaps of 40 μm between carbon electrodes of 25 μm diameter and aspect ratio around 3.6. The fabrication of arrays of SU-8 posts taller than 200 μm with gaps in between narrower than 10 μm proves challenging due to diffraction effects during exposure of thick SU-8 layers and to stiction between structures during drying (data not shown).

The shrinkage obtained at all dimensions is slightly less than isometric. The ratio between the aspect ratio (AR) of SU-8 structures and their correspondent carbon (AR_{carbon}/AR_{SU-8}) is shown in figure 2B. The shrinkage is isometric, 100% symmetric, when the height and diameter of the post shrink in the same proportion (solid line). The shrinkage of the SU-8 pillars fabricated here is slightly less in diameter than in height as concluded by the experimental data points around the 90% shrinkage symmetry line in figure 2B. This result is due to the adhesion force that competes with the shrinkage force at the interface between the substrate and the SU-8 pattern and prevents further shrinkage of the post diameter. Free-standing SU-8 structures shrink isometrically [28].

3.2 Applications of carbon electrodes in DEP

3.2.1 Particle positioning

The most basic DEP function is the selective positioning of particles at specific locations. Particles can be confined to regions of high electric field gradient using a positive DEP force, or pDEP, or to regions of low electric field gradient using a negative DEP force, or nDEP. A

positive DEP force on a particle arises when the complex permittivity of the targeted particle is higher than that of the suspending medium. A negative DEP force is present otherwise. Complex permittivity depends on the frequency of the electric field and a particle may be attracted to pDEP regions at one frequency but repelled to nDEP at another frequency value even when the suspending media remains the same. The pDEP and nDEP regions of a selected carbon-electrode array have been previously modeled [25] and are experimentally proven here using latex particles (sample #1) and *drosophila melanogaster* cells (sample #5). Results are shown in figure 3. Latex particles are selectively confined to nDEP regions (figure 3A), those furthest away from the electrode surface, using a polarizing signal of frequency 10 MHz while *drosophila melanogaster* cells are confined to pDEP regions (figure 3B), those around the electrodes, using a signal of 1 MHz. The magnitude of the signal is 20 V_{pp} in both cases. Applications of cell positioning include analysis of cell networks [29], drug screening [30] and tissue engineering [31]. The addition of a flow in the channel introduces a force (drag) that competes with the DEP force and expands the applications of cell positioning since more complex functions such as filtering and focusing can be implemented.

3.2.2 High throughput filter

Similar carbon-DEP devices but featuring electrodes of different height were used to filter targeted particles out of a mix. First, yeast cells were separated from latex beads at different flow rates. The experimental sample used is #3 in table 2. The experimental setup is based on a centrifugal microfluidics platform and therefore the flow rate in the channel depends on the rotation speed (data not shown). The carbon-DEP devices used here feature either an array of 40 μm-high or 70 μm-high electrodes inside a 100 μm-high microchannel. Therefore, the carbon

electrodes span either 40 or 70% of the channel height. Carbon electrodes are polarized using a sinusoidal signal with magnitude 20 V_{pp} and frequency of 100 kHz to trap both viable and non viable yeast cells and repel latex particles. Results are shown in figure 4. The filter efficiency is 1 when the sample retrieved after experiment contains only latex particles. The use of electrodes with heights closer to the channel height affords higher trapping efficiency at all flow rates. Filter efficiency of 1 is achieved at flow rates below 3 $\mu l \cdot min^{-1}$ using electrodes covering 70% of the channel height. This threshold is expected to be push upwards as the height of the electrodes matches that of the channel. The filter efficiency decreases as flow rate increases since at higher flow rates the hydrodynamic drag force in the channel start to overcome the DEP trapping force. Filtering is not clearly discerned above flow rates of 30 $\mu l \cdot min^{-1}$. The control base line reveals non-specific trapping of the particles in the device likely due to particle sedimentation and other physical phenomena. The filter efficiency at any given flow rate is directly proportional to the percentage of a channel height an electrode covers. The use of electrodes as tall as the channel affords for an electric field gradient across the bulk of the sample and higher efficiency is achieved. High throughput in filtering bacterial cells using 3D carbon-DEP has also been demonstrated by some of us and our collaborators and is detailed elsewhere [21].

3.2.3 Multi-stage filtering

A general schematic of a multi-stage filter is presented in figure 5A. Different electrode array geometries are sequentially positioned inside a microchannel. These array geometries can feature different electrode shapes, sizes and gaps in between them according to the particle targeted in each case. The different arrays can be electrically independent and may be polarized with different signals. The goal of this system is to sort several particle populations by first selectively

trapping targeted populations at different spatial locations and then methodically release and collect each particle population.

The proof-of-concept of a 2-stage filter is implemented here. The experimental sample used is #4 in table 2 and contains latex particles and viable and non viable yeast. Most yeast cells are expected to become non viable after extended immersion (>10 min) in DI water. The experimental setup is that based on a syringe pump described above. The sample is flowed through the carbon electrode arrays at 10 $\mu l \cdot min^{-1}$ while the first electrode array in the path of the sample is polarized using a 5 MHz, 10 V_{pp} sinusoidal signal to trap viable yeast cells. The second array is polarized by a 10 V_{pp}, 500 kHz signal to trap both viable and non viable yeast. Latex particles are never trapped and are continuously collected at the channel outlet. The results are shown in figure 5B. Viable yeast cells are trapped in the first array (shown on the left) while non viable cells are trapped in the second (shown on the right). The sharp difference on the number of cells trapped in each array is due to the fact that most yeast cells are rendered non viable after extended immersion in DI water. The populations of viable and non viable yeast are separated by first releasing and collecting the non viable yeast from the second array and then release and collect the viable yeast trapped in the first array. Three different populations: latex, non viable and viable yeast cells are then separated. Ongoing work is on the quantification of the separation efficiency.

3.2.4 Continuous sorting

Cell focusing using negative DEP is a common methodology for continuous cell sorting [32-34]. This capability is expanded here by demonstrating cell focusing using positive-DEP. The principle works when the hydrodynamic force slightly overcomes the positive-DEP trapping

force. No trapping is necessary but just a positive-DEP force strong enough to attract the targeted cell close to the electrodes. A similar approach was previously demonstrated by Cummings using iDEP [35]. The experimental sample used here is #2 in table 2. The electrode array is polarized using a 10 V_{pp}, 10 MHz sinusoidal signal to attract yeast cells to the surface of the electrodes. The sample flow rate is 5 $\mu l \cdot min^{-1}$. Under these conditions yeast cells are attracted towards the surface of the electrodes but instead of getting trapped they are eluted in a direction co-linear with the positive-DEP regions in the electrode array as shown in figure 6. This is because laminar flow is established in the channel and the flow pathlines are minimally disturbed by the geometry of the carbon electrode array [24]. The use of a 3D electrode array penetrating the bulk of the sample allows for the creation of several simultaneous streams of sorted cells using either negative- or positive-DEP and increases the throughput of the system. This compares advantageously to the use of 3D electrodes positioned only on the channel walls where only up to three simultaneous streams can be created (one using negative-DEP and two using positive-DEP). The experimental module presented here can enable continuous cell sorting using simultaneous positive- and negative-DEP focusing and opens a way for the processing of large sample volumes in short times. Ongoing work is on the fabrication of retrieval geometries positioned at the exit of the electrode array and on the quantification of the efficiency when sorting viable from non viable yeast cells.

4 Concluding remarks

The goal of this work is a high throughput system for bioparticle sorting. The use of 3D electrodes penetrating the sample volume minimizes the distance from a targeted particle to the nearest electric field gradient and improves the throughput of the system. Glass-like carbon

electrodes are more electrochemically stable than metal ones and thus afford the application of higher voltages across the sample without electrolyzing it. Ongoing work is on the fabrication of even taller carbon electrodes (>100 μm) with optimized dimensions to increase trapping volume. The capacity of a carbon-DEP device can also be expanded by increasing the lateral dimensions of the array but an undesired increase of the footprint will come as well. An important improvement presented here is the fabrication of carbon electrodes on a transparent substrate. This facilitates experiment visualization and opens the possibility of incorporating measurement modules such as spectrophotometers to constantly monitor the performance of the device. The fabrication of carbon-DEP devices as detailed here is relatively simple and inexpensive as it only requires photolithography and heat treatment. No metal processing, *i.e.* sputtering, evaporation or electroplating, is required. Shrinkage during pyrolysis is observed to be dependent on the dimensions of the initial SU-8 structure. As detailed above, shrinkage can be an important obstacle when narrow gaps between electrodes are desired. Shrinkage is highly reproducible and the results presented here serve as a practical tool for designing future devices.

A potential disadvantage of carbon-DEP is the electrical resistivity of glass-like carbon which is four orders of magnitude more than that of gold. The voltage loss that develops from the ohmic resistance in the narrow leads connecting the base of the electrodes and the function generator makes it necessary to use higher voltage levels than those used in metal-electrode DEP. However, a voltage in the range of tens of volts has been demonstrated to be sufficient to create a suitable DEP force to manipulate eukaryotic cells when using carbon electrodes. Precious metals are significantly more expensive than polymers used as carbon precursors and the real need for metal connecting leads must be assessed depending on the application. For example, the need for gaps between electrodes less than 20 μm would require the connecting leads to be quite narrow.

At such dimensions, the ohmic resistance of carbon leads can require the use of hundreds of volts and the use of metal leads can be highly beneficial. Preliminary results obtained by some of us show poor adhesion of glass-like carbon to chromium, gold and titanium (data not published). Another potential disadvantage in carbon-DEP is the cost of the fused silica substrate, especially when compared to the cost of float glass substrates commonly used in metal-electrode DEP or the cost of polymers used in iDEP. However, a single substrate, *i.e.* a 4" wafer, can lead to several experimental devices and the impact of the high cost of the substrate can be minimized. In conclusion, carbon-DEP benefits from the fact that only requires the use of tens of volts to implement a suitable electric field gradient for most DEP applications and that high-throughput carbon-DEP devices featuring highly electrochemically stable volumetric electrodes can be fabricated at low cost.

Acknowledgements

Yeast cultures were kindly provided by David Smith from EXIQON in Tustin, CA. Cultures of *Drosophila melanogaster S2* were kindly provided by Luette Forrest at UC Irvine.

Notes

[§] The IUPAC (International Union of Pure and Applied Chemistry) has suggested the use of the term glass-like carbon to refer to carbonaceous materials derived through the pyrolysis of organic polymers. Glass-like carbon is preferred over glassy or vitreous carbon since the latter have been previously introduced as trademarks [36].

[†] A final temperature of 900 °C is expected to yield 95% carbon. The percentage of carbon can be increased to 99% by implementing a final temperature above 1500 °C.

5 References

[1] Gascoyne, P., Vykoukal, J., *Proceedings of the IEEE* 2004, *92*, 22-42.
[2] Pethig, R., Menachery, A., Pells, S., De Sousa, P., *Journal of biomedicine & biotechnology* 2010, *2010*, 182581.
[3] Markx, G. H., Huang, Y., Zhou, X. F., Pethig, R., *Microbiology* 1994, *140*, 585-591.
[4] Wang, L., Flanagan, L. A., Jeon, N. L., Monuki, E., Lee, A. P., *Lab on a Chip* 2007, *7*, 1114-1120.
[5] Voldman, J., Gray, M. L., Toner, M., Schmidt, M. A., *Analytical Chemistry* 2002, *74*, 3984-3990.
[6] Cummings, E. B., Singh, A. K., *Analytical Chemistry* 2003, *75*, 4724-4731.
[7] Lapizco-Encinas, B. H., Simmons, B. A., Cummings, E. B., Fintschenko, Y., *Analytical Chemistry* 2004, *76*, 1571-1579.
[8] Simmons, B. A., McGraw, G. J., Davalos, R. V., Fiechtner, G. J., Fintschenko, Y., Cummings, E. B., *MRS Bulletin* 2006, *31*, 120-124.
[9] Wang, C., Jia, G., Taherabadi, L. H., Madou, M. J., *Journal of Microelectromechanical Systems* 2005, *14*, 348-358.
[10] Blaedel, W. J., Jenkins, R. A., *Analytical Chemistry* 1974, *46*, 1952-1955.
[11] Zittel, H. E., Miller, F. J., *Analytical Chemistry* 1965, *37*, 200-203.
[12] Kim, J., Song, X., Kinoshita, K., Madou, M. J., White, R., *Journal of The Electrochemical Society* 1998, *145*, 2314-2319.
[13] Taylor, R. J., Humffray, A. A., *Jorunal of Electroanalytical Chemistry* 1973.
[14] Van der Linden, W. E., Dieker, J. W., *Analytica Chimica Acta* 1980, *119*, 1-24.
[15] Maropis, P. S., Molinari, J. A., Appel, B. N., Baumhammers, A., *Oral surgery, oral medicine and oral pathology* 1977, *43*, 506-512.
[16] Turon Teixidor, G., Gorkin Iii, R. A., Tripathi, P. P., Bisht, G. S., Kulkarni, M., Maiti, T. K., Battacharyya, T. K., Subramaniam, J. R., Sharma, A., Park, B. Y., Madou, M., *Biomedical Materials* 2008, *3*, 034116.
[17] Cowlard, F. C., Lewis, J. C., *Journal of Materials Science* 1967, *2*, 507-512.
[18] Pesin, L. A., *Journal of Materials Science* 2002, *37*, 1-28.
[19] Park, B. Y., Taherabadi, L., Wang, C., Zoval, J., Madou, M. J., *Journal of the Electrochemical Society* 2005, *152*, J136-J143.
[20] Martinez-Duarte, R., Rouabah, H. A., Green, N. G., Madou, M., Morgan, H., *Eleventh International Conference on Miniaturized Systems for Chemistry and Life Science, uTAS*, Paris, France 2007, pp. 826-828.
[21] Jaramillo, M., Torrents, E., Martinez-Duarte, R., Madou, M., Juarez, A., *Electrophoresis* 2010, *31*, 2921-2928.
[22] Martinez-Duarte, R., Gorkin, R., Abi-Samra, K., Madou, M., *Lab on a Chip* 2010, *10*, 1030-1043.
[23] Park, B. Y., Madou, M. J., *Electrophoresis* 2005, *26*, 3745-3757.
[24] Martinez-Duarte, R., Cito, S., Collado-Arredondo, E., Martinez, S. O., Madou, M. J., *Sensors & Transducers Journal* 2008, *3*, 25-36.
[25] Martinez-Duarte, R., Ph.D., *Mechanical and Aerospace Engineering*, University of California, Irvine, Irvine 2010.
[26] Fitzer, E., *Angewandte Chemie (International ed. in English)* 1980, *19*, 375-385.
[27] Fitzer, E., Schäfer, W., *Carbon* 1970, *8*, 353-364.

[28] Martinez-Duarte, R., M.S., *Mechanical and Aerospace Engineering*, University of California, Irvine, Irvine 2009.
[29] Prasad, S., Yang, M., Zhang, X., Ozkan, C. S., Ozkan, M., *Biomedical Microdevices* 2003, *5*, 125-137.
[30] Hoettges, K. F., Hubner, Y., Broche, L. M., Ogin, S. L., Kass, G. E. N., Hughes, M. P., *Analytical Chemistry* 2008, *80*, 2063-2068.
[31] Markx, G. H., *Organogenesis* 2008, *4*, 11-17.
[32] Wang, L., Lu, J., Marukenko, S. A., Monuki, E. S., Flanagan, L. A., Lee, A. P., *Electrophoresis* 2009, *30*, 782-791.
[33] Demierre, N., Braschler, T., Muller, R., Renaud, P., *Sensors and Actuators, B: Chemical* 2008, *132*, 388-396.
[34] Gascoyne, P. R. C., *Analytical Chemistry* 2009, *81*, 8878-8885.
[35] Cummings, E. B., *IEEE Engineering in Medicine and Biology Magazine* 2003, *22*, 75-84.
[36] Fitzer, E., Kochling, K. H., Boehm, H. P., Marsh, H., *Pue and applied chemistry* 1995, *67*, 473-506.

Table 1 Processing parameters for selected SU-8 structures used in the fabrication of carbon-DEP devices. An acceleration of 100 rpm·s^{-1} is used in all spin coating processes unless noted.

SU-8 type	Spin coating			Soft Bake (min)	Exposure (mJ·cm^{-2})	PEB @ 95 °C (min)	Develop in PGMEA (min)	Hard Bake @ 190 °C (min)	T_{SU-8} (μm)	T_{carbon} (μm)
	# step	speed (rpm)	time (s)							
GM1040	1	500	10	10 @ 95 °C	200	30	30 s	10	2.1	n/a [$]
	2	1600	40							
GM1060	1	500	10	30 @ 95 °C	215	20	1	15	9.2	1.54
	2	2500	40							
GM1070	1	500	10	30 @ 120 °C	150	40	5	n/a [#]	51	17.5
	2	1700	40							
GM1070	1	500	10	45 @ 120 °C	200	70	7	n/a	113	50
	2	900	60							
GM1075	1	850	100	35 @ 120 °C	195	60	8	n/a	150 ± 10 [¶]	72 ± 5
	2[*]	1850	1							
GM1075	1	700	100	45 @ 120°C	200	60	10	n/a	202 ± 10	98 ± 5
	2[*]	1700	1							

Notes: [$] this layer is fabricated around the carbon electrodes at the end of the process and it is not carbonized.

[#] a hard bake is only used for the planar layer, 3D structures are fabricated on top of the first layer.

[*] an acceleration of 1000 rpm·s^{-1} is used in these steps.

[¶] thickness uniformity is not ideal when spin coating GM1075 at such low speeds

T_{SU-8} = thickness of the SU-8 layer. T_{carbon} = thickness of the carbon layer

Table 2 Experimental samples used in this work. A conductivity meter (Oakton CON510 Series or Corning 441) is used to obtain the conductivity of the samples.

Sample	Particles	Media	σ (μS·cm^{-1})	Concentration
1	8 μm-diameter latex particles	DI water	10	1 X 10^6 particles per ml
2	Yeast cells (S. cerevisiae)	0.6 wt% peptone	510	5.1 X 10^7 cells per ml.
3	Yeast cells (*S. cerevisiae*) + 8 μm-diameter latex particles	0.1 wt% BSA	31.2	2.75 X 10^5 particles per ml 40% yeast cells 60% latex particles
4	Yeast cells (*S. cerevisiae*) + 8 μm-diameter latex particles	DI water	8	2 X 10^6 particles per ml 91.3% yeast cells 8.7% latex particles
5	*Drosophila melanogaster* S2	0.1wt% BSA 8.6% sucrose 0.3%dextrose	60	5 X 10^5 cells per ml

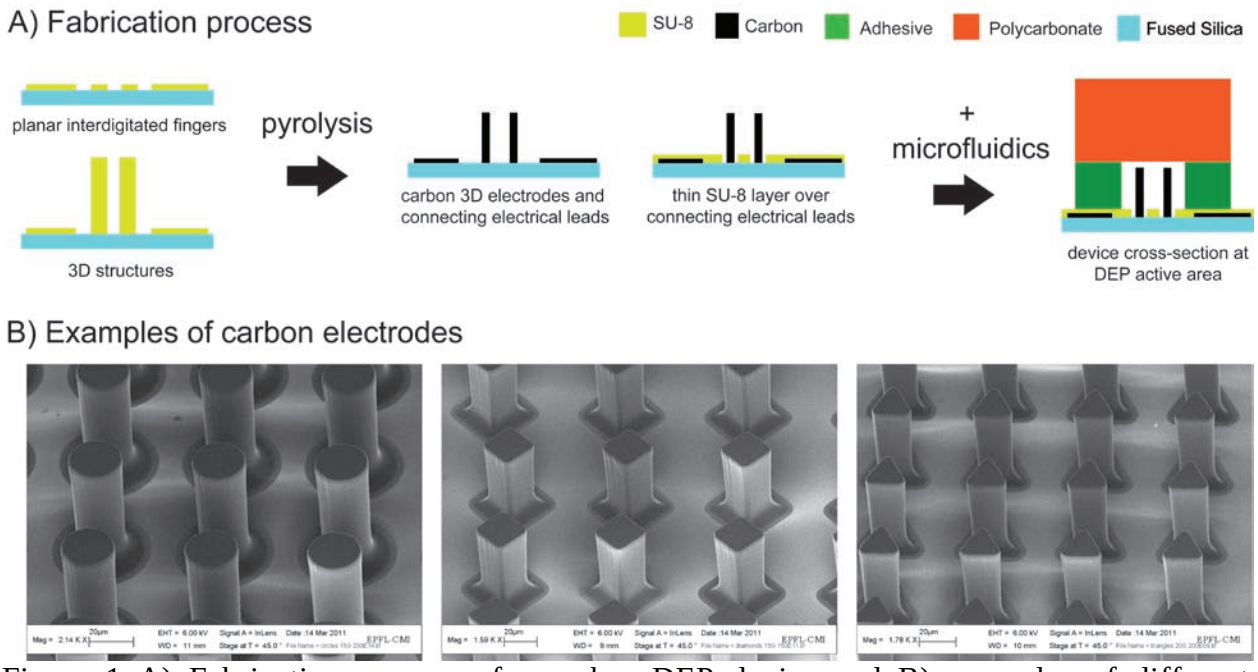

Figure 1 A) Fabrication process of a carbon-DEP device and B) examples of different shapes of carbon electrodes

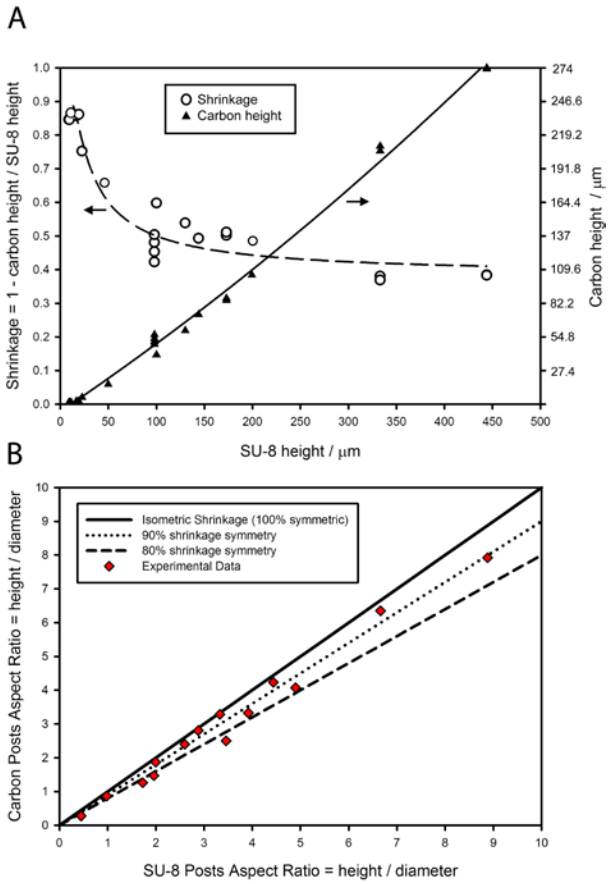

Figure 2 A) Shrinkage percentage (left axis) and carbon height (right axis) as the height of the precursor SU-8 structure increases. The shrinkage percentage depending on the height of the SU-8 structure is plotted as a dashed line fitted to experimental points (rings). The solid line represents the height of the carbon structures depending on the height of the SU-8 pillar and is also fitted to experimental points (triangles). B) Symmetry of shrinkage when pyrolyzing SU-8 on a substrate

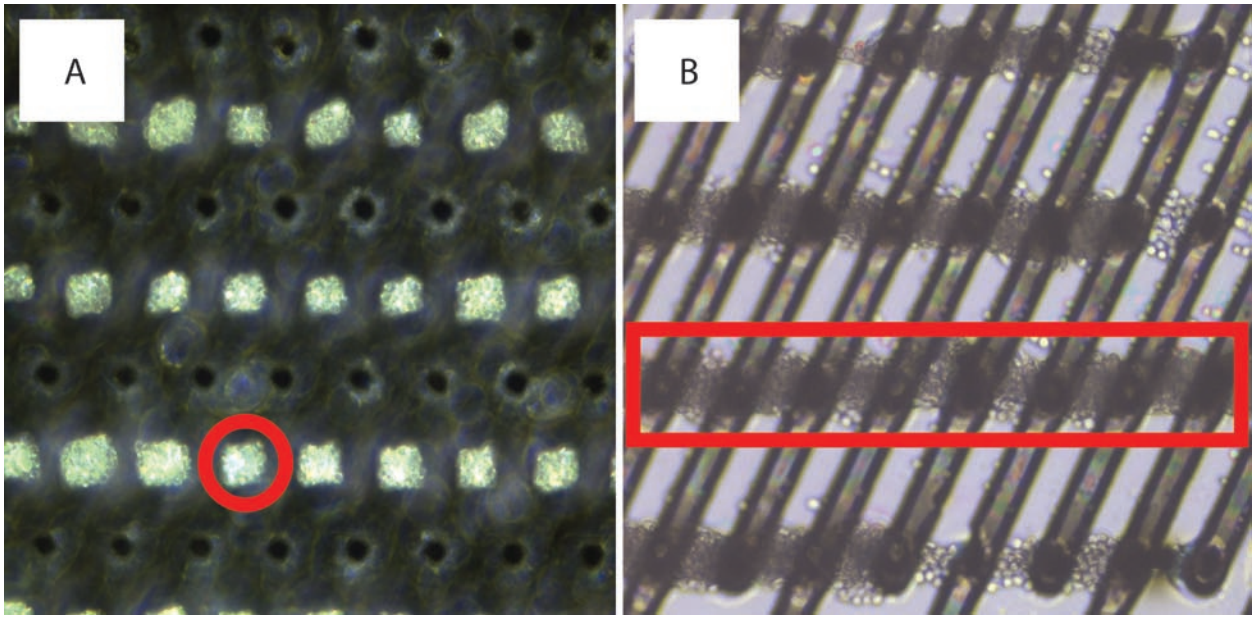

Figure 3 Particle positioning using carbon-DEP: A) latex particles clustered inside negative-DEP regions (circle) between the electrodes (dark circles). B) *Drosophila* cells contained in positive-DEP regions (rectangle) around the electrodes

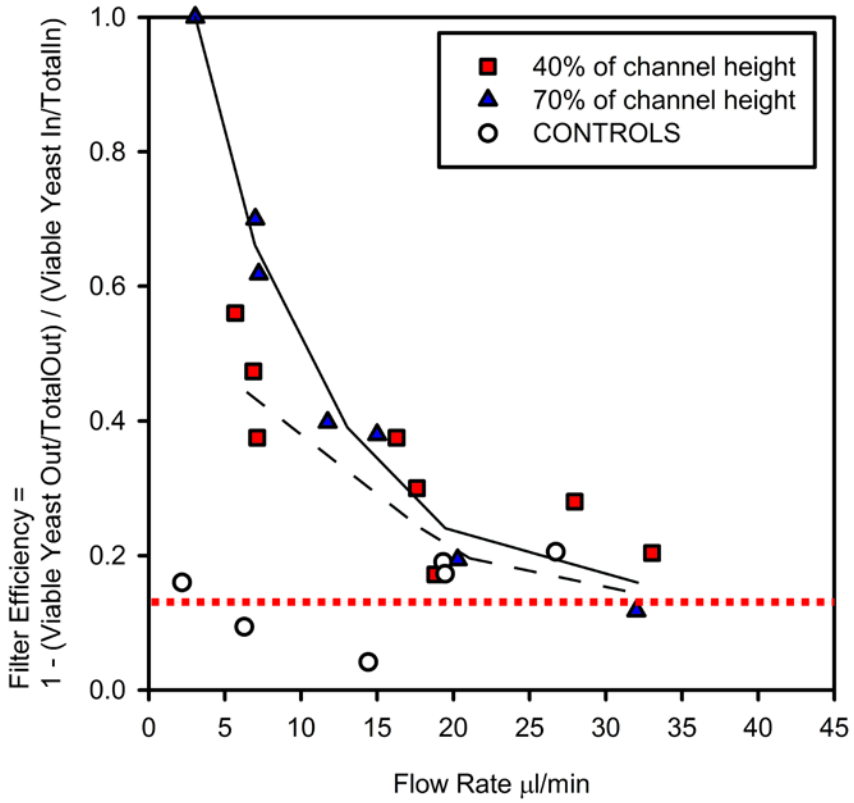

Figure 4 Filter efficiency when separating yeast cells from latex particles using 40 µm-high (40%) or 70 µm-high (70%) electrodes inside a 100 µm-high channel. Electrodes are not polarized during control experiments. Lines are manually fitted to the experimental data

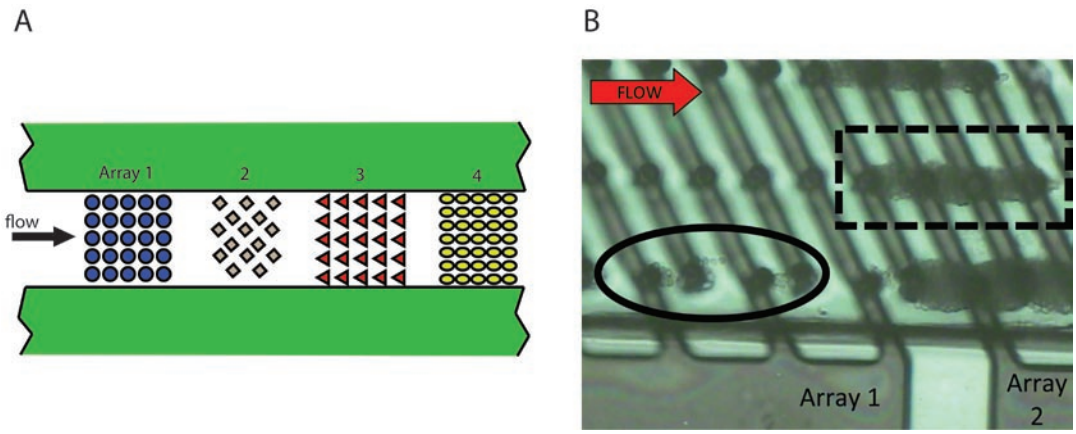

Figure 5 A) General schematic of a multi-stage filter showing 4-stages contained in a microchannel. Each stage is electrically independent and can be polarized using different signals. B) Viable yeast trapped in array 1 (ellipse) while non viable yeast cells are trapped in array 2 (rectangle)

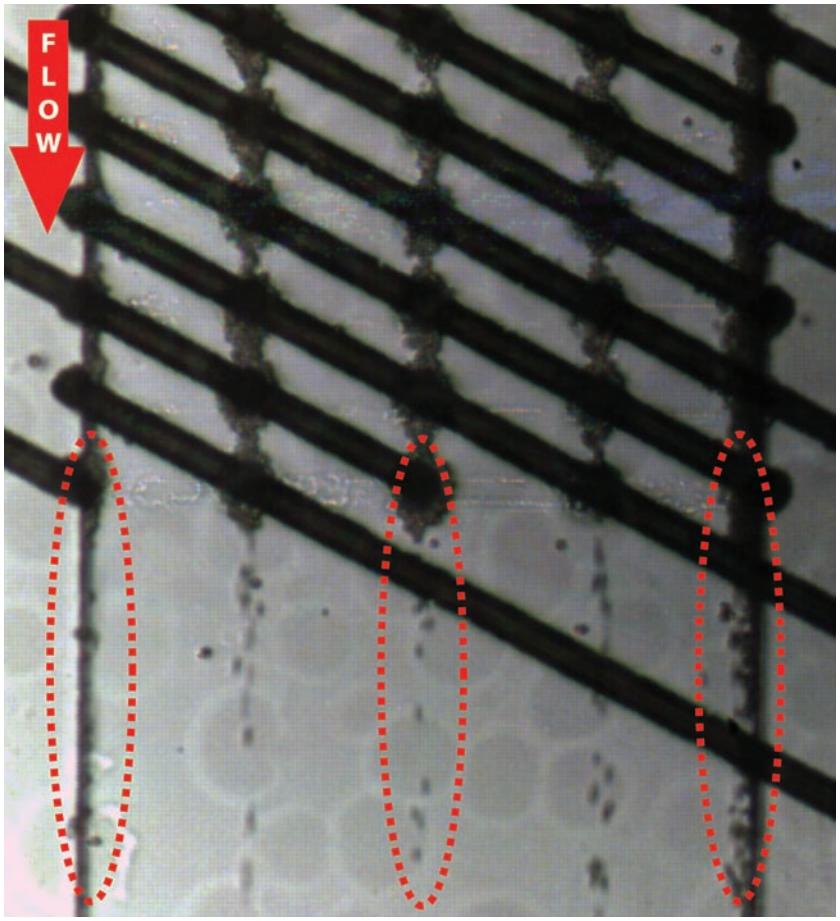

Figure 6 Yeast cells focused into characteristic lines using positive-DEP (red ellipses)